Peristaltic elastic instability in an inflated cylindrical channel

Nontawit Cheewaruangroj

Cavendish Laboratory, University of Cambridge, 19 JJ Thomson Avenue, Cambridge CB3 0HE, United Kingdom

Karolis Leonavicius and Shankar Srinivas

Department of Physiology Anatomy and Genetics, University of Oxford, Oxford OX1 3QX, UK

John S. Biggins

Department of Engineering, University of Cambridge,
Trumpington St, Cambridge CB2 1PZ, United Kingdom

(Dated: January 11, 2019)

A long cylindrical cavity through a soft solid forms a soft microfluidic channel, or models a vascular capillary. We observe experimentally that, when such a channel bears a pressurized fluid, it first dilates homogeneously, but then becomes unstable to a peristaltic elastic instability. We combine theory and numerics to fully characterize the instability in a channel with initial radius a through an incompressible bulk neo-Hookean solid with shear modulus μ. We show instability occurs supercritically with wavelength $12.278....a$ when the cavity pressure exceeds $2.052....\mu$. In finite solids, the wavelength for peristalsis lengthens, with peristalsis ultimately being replaced by a long-wavelength bulging instability in thin-walled cylinders. Peristalsis persists in Gent strain-stiffening materials, provided the material can sustain extension by more than a factor of six. Although naively a pressure driven failure mode of soft channels, the instability also offers a route to fabricate periodically undulating channels, producing, for example, waveguides with photonic/phononic stop bands.

A channel through a soft solid is the prototypical element of biological plumbing [1], guiding fluid through the vascular, lymphatic, digestive, reproductive, renal and respiratory systems. Soft channels also underpin the blossoming field of soft microfluidics [2], which exploits the convenience of soft lithography for rapid prototyping [3, 4], the deformability of soft channels to actuate valves and pumps [2, 5, 6], and the mechanical compatibility between soft solids and soft tissues to build organs-on-chips and medical implants [7, 8]. Here we investigate how soft channels deform as their internal pressure increases. Thin-walled elastic tubes famously undergo long-wavelength bulging, bending and ballooning instabilities [9–18] under inflation, but a channel through a bulk solid arises in the opposite (divergently thick walled) limit. We combine theory, numerics and experiment (Fig. 1) to show that, while modest fluid pressure causes simple dilation, the channel undergoes a finite-wavelength elastic instability and adopts a peristaltically undulating morphology when the pressure becomes comparable to the solid's shear modulus,

The hallmark of soft solids, including elastomers, gels, and many biological tissues, is that they can sustain geometrically large elastic strains ($\gtrsim 100\%$) without failing, exposing them to the full complexity of large deformation geometry. This generates a range of geometrically motivated elastic instabilities, including buckling [19], creasing [20–25] and wrinkling [26, 27] under compression; fingering [28–32], fringing [33, 34] and beading [35–38] under tension; and ballooning [9, 13, 16, 18, 39], aneurysm [39, 40] and cavitation [41–43] under inflation. These instabilities are important failure modes [44], but have also
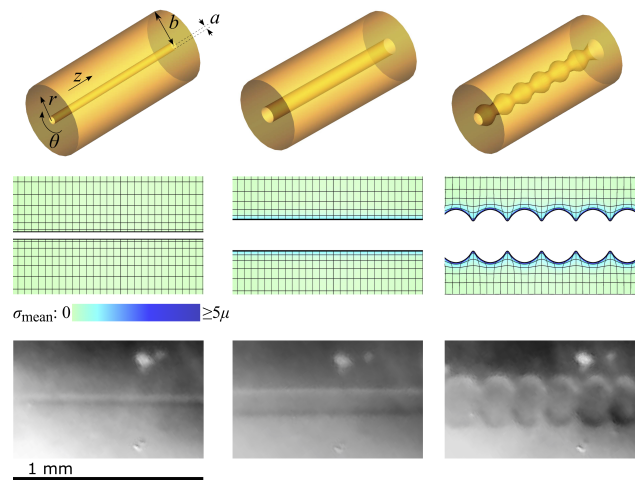

FIG. 1. Schematic (top), numerics (middle, neo-Hookean) and experiment (bottom, polyacrylamide) showing the shape evolution of a cylindrical channel through a soft solid under increasing internal pressure. At modest pressure the channel dilates simply, but at high pressures it undergoes an elastic instability and adopts a peristaltic shape (right).

been exploited by evolution to sculpt developing brains [45, 46], guts [47, 48] and other organs [49–53], and by engineers to make shape-switching devices [54–57].

We start by considering a cylindrical cavity, with initial radius a, running through soft elastic material occupying $a < r < b$, as shown in Fig. 1. If the channel is subject to an internal pressure P_{in}, it will dilate, deforming the solid and causing it to store elastic energy E_{el}. The

observed dilation will be determined by the minimum of the effective energy

$$E_{tot} = E_{el} - P_{in}V, \tag{1}$$

where V is the dilated channel's volume. If the deformed solid has displacement $\mathbf{u}$, its local shape change is described by the deformation gradient tensor $F = I + \nabla\mathbf{u}$ (I being the identity matrix, and ∇ the gradient operator) and its elastic energy density is of the form $W(F)$. We model the solid as an incompressible ($\text{Det}(F) = 1$) neo-Hookean material [58] with shear modulus μ, requiring $W(F) = \frac{1}{2}\mu\text{Tr}(F \cdot F^T) - P(\text{Det}(F) - 1)$ where P is a Lagrange multiplier pressure field enforcing incompressibility. This model is exact for Gaussian polymer networks, and valid until deformations of several hundred percent in lightly cross-linked gels/elastomers [59] including our polyacrylamide gels [60]. It is also the simplest large-deformation elastic model, and correspondingly offers the clearest exposition of geometrically motivated instabilities.

Minimizing E_{tot} with respect to variations in $\mathbf{u}$ and P gives the expected equations of mechanical equilibrium, and the constraint of incompressibility,

$$\nabla \cdot \sigma = 0, \quad \text{Det}(F) = 1, \tag{2}$$

where $\sigma = \frac{\partial W}{\partial F} = (\mu F - PF^{-T})$ is the large deformation "first Piola-Kirchhoff" stress, a two-point tensor relating forces in the deformed configuration to reference configuration areas. These equations are augmented by the natural inner and outer boundary conditions:

$$(\sigma + P_f F^{-T}) \cdot \hat{\mathbf{r}}\big|_{r=a,b} = 0, \tag{3}$$

where the boundary fluid pressure $P_f = P_{in}, 0$ at $r = a, b$ respectively, and $\hat{\mathbf{r}}$ is the radial unit vector.

We first consider a simple radial dilation: $\mathbf{u} = u_0(r)\hat{\mathbf{r}}$, $P = \mu P_0(r)$. Incompressibility requires

$$R \equiv r + u_0(r) = \sqrt{c^2 + r^2}, \tag{4}$$

where the constant of integration, c, parameterizes the degree of cavity dilation, with the inner radius rising by a factor of $\lambda = \sqrt{1 + c^2/a^2}$. Mechanical equilibrium ($\nabla \cdot \sigma = 0$) then gives the form of the pressure field which, taking account of the stress-free outer boundary, is

$$P_0 = \frac{1}{2}\left[\frac{r^2}{c^2 + r^2} + \frac{b^2}{c^2 + b^2} + \ln\left(\frac{b^2(c^2 + r^2)}{r^2(c^2 + b^2)}\right)\right]. \tag{5}$$

Finally, the inner boundary condition gives an implicit solution for the channel dilation, λ, which, introducing $g(x) \equiv (1/x) - \log(x)$, can be written

$$P_{in} = \frac{\mu}{2}\left[g\left(1 + (a/b)^2(\lambda^2 - 1)\right) - g\left(\lambda^2\right)\right]. \tag{6}$$

This predicted dilation is plotted for a range of values of a/b in Fig. 2. Dilation rises monotonically with P_{in}, and
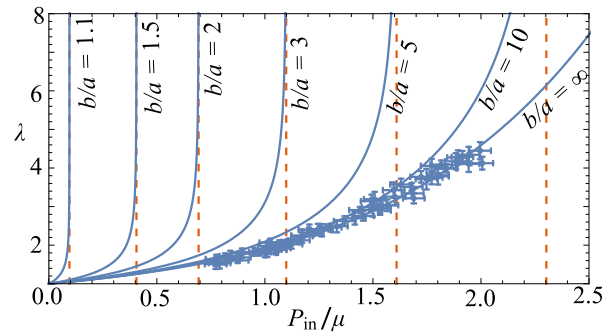

FIG. 2. Dilation factor, λ, of a neo-Hookean cylindrical channel as a function of its interior pressure P_{in}, for a range of aspect ratios b/a. Predicted dilation (solid lines) diverges at $P_{in} = \mu\log(b/a)$ but a channel through a bulk solid ($b \to \infty$) never diverges. Experimental points are individual constant-pressure measurements from three channels through polyacrylamide slabs, reproducing the bulk neo-Hookean theoretical dilation.

diverges at $P_{in} = \mu\log(b/a)$. If $b = a + t \approx a$, (a pipe with thin wall thickness t) this critical pressure reduces to $P_{in} \approx \mu t/a$, the signature scaling of elastic instabilities in membrane tubes [9–18]. Conversely, in the $b \to \infty$ limit eqn. (6) becomes

$$P_{in} = \frac{\mu}{2}\left[1 + \log(\lambda^2) - \lambda^{-2}\right], \tag{7}$$

showing that the channel dilates, but only diverges at infinite pressure. In contrast, the result for a spherical cavity in a bulk solid, $P_{in} = \frac{\mu}{2}\left[5 - 4\lambda^{-1} - \lambda^{-4}\right]$, diverges at $P_{in} = \frac{5}{2}\mu$, a celebrated result known as solid cavitation [41].

We investigated the stability of cylindrical cavities under inflation experimentally by cross-linking a 1mm thick rectangular slab of polyacrylamide gel around a 30 μm wire (see experimental SI for details). The wire was then removed (leaving a cylindrical channel), and the gel was equilibrated in a phosphate buffered saline solution (PBS). Finally, one end of the channel was plugged with a glass bead, and the channel was inflated by pumping additional PBS in through a glass capillary inserted at the other end. We used a computer controlled air pressure source to vary the pressure in the cavity, and monitored the evolving shape of the channel with a CMOS camera sensor fitted to a Leica stereomicroscope eyepiece. As seen in Fig. 2, at modest pressures the channels simply dilates, in good agreement with the prediction for a channel through a bulk neo-Hookean. However, as seen in Fig. 1 and video E1, beyond a critical pressure, the channel adopts a new peristaltically undulating morphology. The transition is reversible, and occurs at quasi-static rates of inflation, suggesting a purely elastic mechanical instability.

To understand this transition, we examine the linear stability of uniform dilation to small perturbations, $\mathbf{u} =$
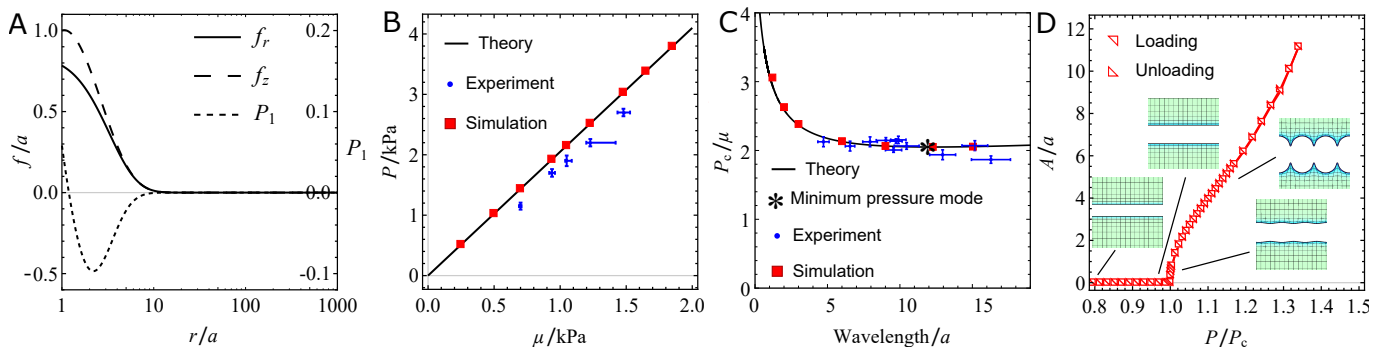
FIG. 3. Theoretical, numerical and experimental treatment of the peristaltic instability in a channel through a bulk solid. (a) Peristaltic fields for the first unstable mode from the stability analysis, plotted against the undeformed coordinate r. (b) Critical pressure for instability as a function of shear modulus. (c) Critical pressure for instability at each wavelength. (d) Simulated amplitude as a function of P_{in}, showing a supercritical transition without hysteresis.

$u_0\hat{\mathbf{r}} + \delta\mathbf{u}$, $P = \mu P_0 + \delta P$, which, in turn, induce first order changes to the deformation gradient ($\delta F = \nabla\delta\mathbf{u}$) and the stress ($\delta\sigma = \mu\delta F - \delta P F_0^{-T} - \mu P_0\delta(\mathrm{Det}\,(F)\,F^{-T})$). Expanding eqns. (2-3) to first order, we see the perturbation must satisfy $\nabla\cdot\delta\sigma = 0$ (mechanical equilibrium), $\mathrm{Tr}(F_0^{-1}\cdot\delta F) = 0$ (incompressibility) and $(\delta\sigma + P_f\delta(\mathrm{Det}\,(F)\,F^{-T}))\cdot\hat{\mathbf{r}}|_{r=a,b} = 0$ (boundary conditions). Substituting a peristaltic form

$$\delta\mathbf{u} = f_r(r)\cos(kz)\hat{\mathbf{r}} + f_z(r)\sin(kz)\hat{\mathbf{z}} \quad (8)$$
$$\delta P = \mu P_1(r)\cos(kz), \quad (9)$$

and using Lagrange's derivative notation, $f' = \frac{\partial f}{\partial r}$, the condition of incompressibility reduces (see theoretical supplement) to

$$R\left(Rf_r' + krf_z\right) + rf_r = 0, \quad (10)$$

the equations of mechanical equilibrium become

$$kf_r\left(r^2 - R^2\right)^2 + rR^3\left(rf_z'' + f_z' - k^2rf_z + krP_1\right) = 0 \quad (11)$$
$$rR^4\left(rf_r'' + f_r' - RP_1'\right) + r^2f_r\left(r^2 - R^2\left(k^2R^2 + 2\right)\right)$$
$$+ kRf_z\left(r^2 - R^2\right)^2 = 0 \quad (12)$$

and the boundary conditions (at both $r = a, b$) become

$$Rf_z' - krf_r = 0 \quad (13)$$
$$rR^2f_r' - r^2f_r - kr^2Rf_z - R^3P_1 = 0. \quad (14)$$

Given $R \equiv r + u_0 = \sqrt{a^2\left(\lambda^2 - 1\right) + r^2}$, equations (10-14) form a fourth order generalized eigensystem for the critical degree of dilation, λ, required for instability. Previous authors have solved this system for modestly thick tubes [15] ($b - a \sim a$) which, like their thin-walled counterparts, first become unstable via long-wavelength modes. Such modes vanish beyond a critical wall thickness, leading these authors to conclude that sufficiently thick pipes

are stable. However, inspired by our experimental observations, we use matlab's bvp4c routine to search, numerically, for finite wavelength solutions ($k \sim 1/a$) in a tube which is sufficiently thick ($b = 1000a$) to approximate a bulk solid. The first unstable mode occurs at $\lambda = 4.824...$ (requiring $P_{in} = 2.052...\mu$) and with finite wavelength $2\pi/k = 12.278...a$. We plot the form of this solution in Fig. 3A, showing the fields take maximum values near the cavity, and only penetrate a distance $\sim 10a$ into the bulk, confirming the outer boundary is effectively at infinity. The variation of threshold pressure with wavelength is plotted in Fig. 3C. Although the resulting threshold curve is very flat, it does have a minimum (indicated with a star) corresponding to the first unstable mode.

In Fig. 3B-C we also compare these predictions with bespoke [45, 61] axisymmetric [38, 62] finite element calculations ($b/a \geq 60$, details in numerical supplement) and threshold measurements obtained in "unloading" experiments, in which a channel is pressurized well beyond the point of instability then quasi-statically depressurized until peristalsis vanishes. In particular, we show in Fig. 3B that both numerical and experimental cavities are indeed unstable above $P_{in} = 2.05...\mu$ over a range of gel moduli [63]. This linearity in gel modulus is the hallmark of a purely elastic instability. In finite elements, long cavities select the expected $2\pi/k = 12.278...a$ wavelength (theory SI Fig. 2), but we can artificially fix the wavelength via periodic boundary conditions. In Fig. 3C, we confirm these alternative wavelengths become unstable at the corresponding (higher) predicted pressures. In experiments, we cannot prescribe a wavelength, but we find the instability naturally occurs with a broad range of wavelengths (a signature of the very flat theoretical wavelength-threshold curve) and, in each case, peristalsis vanishes close to the predicted threshold pressure for that wavelength. The experimental instability is often observed at pressures slightly below the theoretical value,
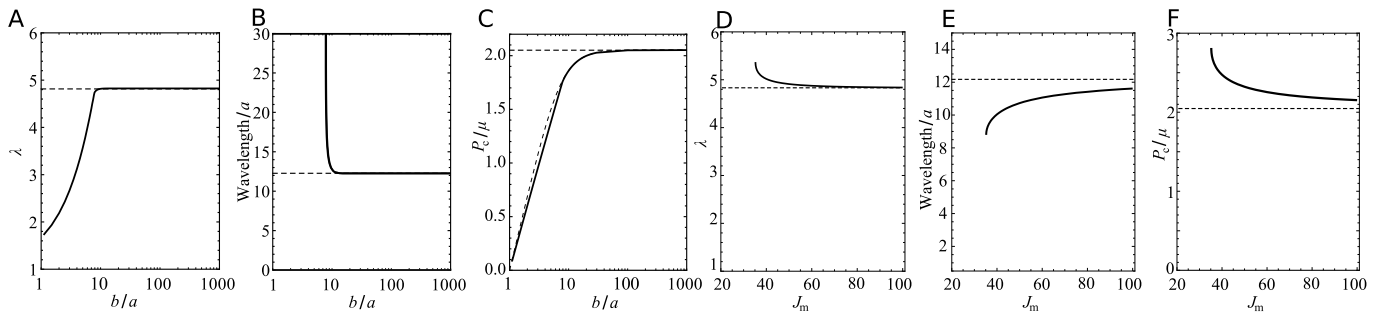
FIG. 4. Effect of finite outer radius (a-c) and finite extensibility (d-f) on the critical dilation (a,d), critical wavelength (b,d) and critical pressure (c,f) of the peristaltic elastic instability. Straight dashed lines indicate the bulk neo-Hookean solution, while solid lines indicated the full finite b/a solution (a-c) and Gent material solution (d-f). The curved dashed line in (c) is the pressure, at finite b/a, required to produce the bulk critical dilation $\lambda = 4.82...$

which we attribute to the finite slab thickness.

Unlike stability analysis, our finite element calculations can explore peristalsis beyond threshold. We conducted a numerical loading/unloading cycle in a bulk solid (Fig. 3D and video N1), which shows the amplitude growing and shrinking continuously above threshold without hysteresis; the instability is supercritical. Repeating this exercise with different wavelengths reveals that the energy-minimizing wavelength lengthens slightly (theory SI Fig. 3) beyond threshold.

Overall, our analysis leads to a simple conclusion: the driver for peristalsis is that, for a given inflated channel volume, the peristaltic form requires less shape change and saves elastic energy. An instructive comparison is to the Plateau-Rayleigh instability [35, 38, 64], in which peristalsis occurs because it reduces a cylinder's surface area, and hence reduces its surface energy. Here, peristalsis will also reduce the channel's inner surface area, relieving the base-state stretch and saving elastic energy. The base-state stretch (4) decays into the bulk over the length scale a, and the energetically optimal peristaltic fields will penetrate this dilated region, where they relieve strain, but not further where they would add strain and cost energy. As is characteristic of oscillating elastic fields, the peristaltic field's penetration distance is set by their wavelength, resulting in an optimal wavelength proportional to a. Since this is a geometric mechanism, we expect peristalsis to be generic in sufficiently deformable elastic channels. In the final section of our study, we investigate how robust peristalsis is to changes in geometry and choice of elastic material.

First, we analyze peristalsis at finite b/a, by numerically solving the stability equations (10-14) to plot threshold pressure vs wavelength in cavities with a range of values of b/a (theory SI Fig. 1). The equations only depend on P_{in} via the dilation (λ) it produces, and only depend on b via the outer boundary condition where the fields are in any event decayed. The instability thus has a universal form in all channels with modestly large b/a

which all become unstable at the bulk wavelength and dilation. In Fig. 4A-B we show the full form of the threshold dilation, and wavelength as a function of b/a. As anticipated, these only deviate from the bulk form when $b/a \lesssim 10$, with wavelength growing and dilation falling in finite systems. However, the critical pressure (Fig. 4C) drops from the bulk value rather earlier, as the pressure required to produce this dilation is reduced in finite systems, in accordance with eqn. (6). Peristalsis is replaced by a long-wavelength axisymmetric bulging instability for $b/a \lesssim 7$, the mode previously identified in thick-walled tubes [15], which sets the ultimate limit of peristalsis in finite systems.

Secondly, we analyze peristalsis beyond Hookean materials. Most elastomers/gels are neo-Hookean at modest strains, but have a finite extensibility, owing to their finite length chains. The resulting stain-stiffening is captured by the Gent model [65], $W(F) = -\frac{1}{2}\mu J_m \log\left(1 - (\mathrm{Tr}\left(F.F^T\right) - 3)/J_m\right) - P(\mathrm{Det}\left(F\right) - 1)$, which reproduces the neo-Hookean energy when the strain measure $\mathrm{Tr}\left(F.F^T\right) - 3$ is small, but diverges when it approaches J_m, a phenomenological parameter encoding finite extensibility. Repeating the bulk linear-stability analysis, we find the base state is identical, whilst the stability equations become more complicated, but still admit numerical solution. We display the critical dilation, wavelength and pressure as a function of J_m in Fig. 4C-E, showing that finite extensibility generates only modest changes in the form of peristalsis, but eliminates the instability entirely for $J_m < 35$, corresponding to materials with limiting uniaxial extension factor of $\lambda \lesssim 6$.

In summary, we have shown that a cylindrical channel through a soft solid will spontaneously adopt a peristaltically undulating shape when bearing a pressure comparable to the solid's shear modulus. The instability takes a simple form in channels through bulk neo-Hookean solids, occurring at a critical pressure ($2.05...\mu$) proportional to the channel shear modulus, and with a wavelength which
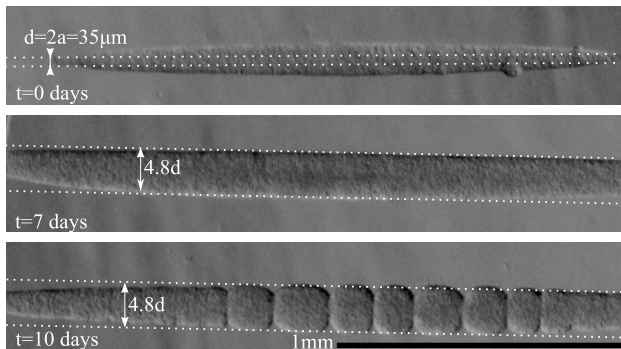
FIG. 5. Instability when an embryonic stem cell tissue grows inside a channel. Dashed lines indicate initial channel diameter $d = 2a$ (top), and predicted threshold diameter for instability (4.8d, middle, bottom).

is a multiple of the cavity radius. Assuming a finite threshold and wavelength, these scalings are an inevitable consequence of the scale invariance of elasticity which means a is the only length scale in the problem, and μ is the only stress scale. Several one-length-scale elastic fingering phenomena produce analogous wavelengths [30–32, 66–69], and solid cavitation of bulk spherical cavities follows the same stress scaling ($P_c = 2.5\mu$), though bulk peristalsis of cylindrical cavities requires less pressure.

Peristalsis is also expected in finite solids, provided $b/a \gtrsim 7$, and strain-stiffening materials provided they are sufficiently deformable. In some less-deformable elastic media, the strain concentrations associated with peristalsis will precipitate fracture and failure, suggesting peristalsis places a fundamental limit on the pressure a channel can bear, just as Euler-buckling limits loading of columns. Conversely, in sufficiently deformable solids, peristalsis offers a route to reversibly introduce periodicity into a channel, potentially allowing a highly reflective photonic/phononic stop-band [70, 71] to be switched within a deformable waveguide.

We speculate that the peristaltic instability will also manifest in biology, sculpting channels during both pathological and developmental processes. Indeed, we first observed peristalsis in hydrogel channels containing growing mouse embryonic stem cell tissues (Fig. 5). More precisely, we injected a dense suspension of murine embryonic stem cells into a 35μm diameter ($a = 17.5\mu$m) channel, which rapidly adhered into a monolithic tissue. This tissue grew for ten days within the channel, nourished by cell culture media ([72, 73] and experimental SI). Such embryonic stem cell tissue is a soft incompressible solid with a finite yield stress, and dilates the channel as it grows. The tissue solidity arises because the cells are both individually elastic (with moduli ~ 100Pa [74]) owing to their cytoskeleton, and adhere to each other by expression of e-cadherin [75]: we found disrupting either aspect (using Cytochalasin D [76] or EDTA [77] respec-

tively, see experimental SI and Fig.3) lead to a tissue which could no longer deform the hydrogel. With the undisrupted culture, peristalsis appeared on day seven, when the central channel dilation achieved the expected threshold of $\lambda \approx 4.8$. As in pressure controlled experiments, peristalsis had uneven wavelengths, varying between $7a$ and $12a$, reflecting the instability's flat dispersion curve.

In biology, one commonly encounters thin-walled tubes through soft tissues. Such tubes can be included in the current framework by adding a thin tube of different elastic material, with modulus $\mu_{\text{tube}} = \eta\mu$, at the inner radius of the channel. Under inflation this system must span from conventional long-wavelength tube instabilities at high η, to finite wavelength peristalsis at low η, and mapping this transition is likely to be a rich and biologically relevant subject for future investigations.

[1] T. Pedley, G. Batchelor, H. Moffat, and M. Worster, Perspectives in fluid dynamics: a collective introduction to current research , 105 (2000).
[2] M. A. Unger, H.-P. Chou, T. Thorsen, A. Scherer, and S. R. Quake, Science **288**, 113 (2000).
[3] Y. Xia and G. M. Whitesides, Annual review of materials science **28**, 153 (1998).
[4] J. C. McDonald, D. C. Duffy, J. R. Anderson, D. T. Chiu, H. Wu, O. J. Schueller, and G. M. Whitesides, ELECTROPHORESIS: An International Journal **21**, 27 (2000).
[5] T. Thorsen, S. J. Maerkl, and S. R. Quake, Science **298**, 580 (2002).
[6] H.-P. Chou, M. A. Unger, and S. R. Quake, Biomedical Microdevices **3**, 323 (2001).
[7] I. E. Araci, B. Su, S. R. Quake, and Y. Mandel, Nature medicine **20**, 1074 (2014).
[8] A. Koh, D. Kang, Y. Xue, S. Lee, R. M. Pielak, J. Kim, T. Hwang, S. Min, A. Banks, P. Bastien, M. C. Manco, L. Wang, K. R. Ammann, K.-I. Jang, P. Won, S. Han, R. Ghaffari, U. Paik, M. J. Slepian, G. Balooch, Y. Huang, and J. A. Rogers, Science Translational Medicine **8**, 366ra165 (2016), http://stm.sciencemag.org/content/8/366/366ra165.full.pdf.
[9] A. Mallock, Proceedings of the Royal Society of London **49**, 458 (1891).
[10] A. H. Corneliussen and R. Shield, Archive for Rational Mechanics and Analysis **7**, 273 (1961).
[11] H. Alexander, International Journal of Mechanical Sciences **13**, 87 (1971).
[12] R. T. Shield, Zeitschrift für angewandte Mathematik und Physik ZAMP **23**, 16 (1972).
[13] R. W. Ogden, Proc. R. Soc. Lond. A **326**, 565 (1972).
[14] D. Haughton and R. Ogden, Journal of the Mechanics and Physics of Solids **27**, 179 (1979).

[15] D. Haughton and R. Ogden, Journal of the Mechanics and Physics of Solids **27**, 489 (1979).

[16] A. Gent, Rubber chemistry and technology **72**, 263 (1999).

[17] Y. Fu, S. Pearce, and K.-K. Liu, International Journal of Non-Linear Mechanics **43**, 697 (2008).

[18] F. Meng, J. Z. Chen, Z. Ouyang, *et al.*, AIChE Journal **60**, 1393 (2014).

[19] L. Euler, Opera omnia I **24**, 231 (1744).

[20] M. Biot, *Mechanics of incremental deformations: theory of elasticity and viscoelasticity of initially stressed solids and fluids, including thermodynamic foundations and applications to finite strain* (Wiley New York:, 1965).

[21] V. Trujillo, J. Kim, and R. C. Hayward, Soft Matter **4**, 564 (2008).

[22] S. Cai, D. Chen, Z. Suo, and R. C. Hayward, Soft Matter **8**, 1301 (2012).

[23] E. Hohlfeld and L. Mahadevan, Physical review letters **106**, 105702 (2011).

[24] J. Dervaux and M. B. Amar, Annu. Rev. Condens. Matter Phys. **3**, 311 (2012).

[25] T. Tallinen, J. S. Biggins, and L. Mahadevan, Physical review letters **110**, 024302 (2013).

[26] H. G. Allen, *Analysis and Design of Structural Sandwich Panels: The Commonwealth and International Library: Structures and Solid Body Mechanics Division* (Pergamon Press, 1969).

[27] E. Cerda and L. Mahadevan, Physical review letters **90**, 074302 (2003).

[28] K. Shull, C. Flanigan, and A. Crosby, Physical Review Letters **84**, 3057 (2000).

[29] B. Saintyves, O. Dauchot, and E. Bouchaud, Physical review letters **111**, 047801 (2013).

[30] J. S. Biggins, B. Saintyves, Z. Wei, E. Bouchaud, and L. Mahadevan, Proceedings of the National Academy of Sciences **110**, 12545 (2013).

[31] S. Mora, T. Phou, J.-M. Fromental, and Y. Pomeau, Physical review letters **113**, 178301 (2014).

[32] J. S. Biggins, Z. Wei, and L. Mahadevan, EPL (Europhysics Letters) **110**, 34001 (2015).

[33] S. Lin, T. Cohen, T. Zhang, H. Yuk, R. Abeyaratne, and X. Zhao, Soft matter **12**, 8899 (2016).

[34] S. Lin, Y. Mao, R. Radovitzky, and X. Zhao, Journal of the Mechanics and Physics of Solids **106**, 229 (2017).

[35] S. Mora, T. Phou, J.-M. Fromental, L. M. Pismen, and Y. Pomeau, Physical review letters **105**, 214301 (2010).

[36] M. Taffetani and P. Ciarletta, Physical Review E **91**, 032413 (2015).

[37] P. Ciarletta and M. B. Amar, Soft Matter **8**, 1760 (2012).

[38] C. Xuan and J. Biggins, Physical Review E **95**, 053106 (2017).

[39] H. Alexander, International Journal of Engineering Science **9**, 151 (1971).

[40] A. Gent, International Journal of Non-Linear Mechanics **40**, 165 (2005).

[41] A. Gent and P. Lindley, Proc. R. Soc. Lond. A **249**, 195 (1959).

[42] J. M. Ball, Phil. Trans. R. Soc. Lond. A **306**, 557 (1982).

[43] A. N. Gent, Rubber Chemistry and Technology **63**, 49 (1990).

[44] A. E. HIRST JR, J. VARNER J JOHNS, and S. W. KIME JR, Medicine **37**, 217 (1958).

[45] T. Tallinen, J. Y. Chung, J. S. Biggins, and L. Mahadevan, PNAS **111**, 12667 (2014).

[46] T. Tallinen, J. Y. Chung, F. Rosseau, N. Girard, J. Lefevre, and L. Mahadevan, Nature Phys. **12**, 588 (2016).

[47] T. Savin, N. A. Kurpios, A. E. Shyer, P. Florescu, H. Liang, L. Mahadevan, and C. J. Tabin, Nature **476**, 57 (2011).

[48] A. E. Shyer, T. Tallinen, N. L. Nerurkar, Z. Wei, E. S. Gil, D. L. Kaplan., C. J. Tabin, and L. Mahadevan, Science **342**, 212 (2013).

[49] J. Dervaux, Y. Couder, M.-A. Guedeau-Boudeville, and M. B. Amar, Physical review letters **107**, 018103 (2011).

[50] P. Ciarletta and M. B. Amar, International Journal of Non-Linear Mechanics **47**, 248 (2012).

[51] M. Kücken and A. Newell, EPL (Europhysics Letters) **68**, 141 (2004).

[52] M. Diab, T. Zhang, R. Zhao, H. Gao, and K.-S. Kim, Proc. R. Soc. A **469**, 20120753 (2013).

[53] M. J. Razavi, R. Pidaparti, and X. Wang, Physical Review E **94**, 022405 (2016).

[54] J. Shim, C. Perdigou, E. R. Chen, K. Bertoldi, and P. M. Reis, Proceedings of the National Academy of Sciences **109**, 5978 (2012).

[55] D. Yang, B. Mosadegh, A. Ainla, B. Lee, F. Khashai, Z. Suo, K. Bertoldi, and G. M. Whitesides, Advanced Materials **27**, 6323 (2015).

[56] J. Marthelot, P.-T. Brun, F. L. Jiménez, and P. M. Reis, Physical Review Materials **1**, 025601 (2017).

[57] D. Wang, N. Cheewaruangroj, Y. Li, G. McHale, Y. Jiang, D. Wood, J. S. Biggins, and B. B. Xu, Advanced Functional Materials **28** (2018).

[58] R. S. Rivlin, Philosophical Transactions of the Royal Society of London A: Mathematical, Physical and Engineering Sciences **240**, 459 (1948).

[59] H. M. James and E. Guth, The Journal of Chemical Physics **11**, 455 (1943).

[60] J. Tang, J. Li, J. J. Vlassak, and Z. Suo, Extreme Mechanics Letters **10**, 24 (2017).

[61] T. Tallinen and J. S. Biggins, Physical Review E **92**, 022720 (2015).

[62] C. Xuan and J. Biggins, Physical Review E **94**, 023107 (2016).

[63] J. R. Tse and A. J. Engler, Current protocols in cell biology , 10 (2010).

[64] L. Rayleigh, Proceedings of the London mathematical society **1**, 4 (1878).

[65] A. Gent, Rubber chemistry and technology **69**, 59 (1996).

[66] A. Ghatak and M. K. Chaudhury, Langmuir **19**, 2621 (2003).

[67] M. Adda-Bedia and L. Mahadevan, in *Proceedings of the Royal Society of London A: Mathematical, Physical and Engineering Sciences*, Vol. 462 (The Royal Society, 2006) pp. 3233–3251.

[68] M. K. Chaudhury, A. Chakrabarti, and A. Ghatak, The European Physical Journal E **38**, 82 (2015).

[69] J. S. Biggins and L. Mahadevan, Soft matter **14**, 7680 (2018).

[70] L. Rayleigh, The London, Edinburgh, and Dublin Philosophical Magazine and Journal of Science **26**, 256 (1888).

[71] K. Bertoldi and M. Boyce, Physical Review B **77**, 052105 (2008).

[72] J. M. Rhee, M. K. Pirity, C. S. Lackan, J. Z. Long, G. Kondoh, J. Takeda, and A.-K. Hadjantonakis, Genesis **44**, 202 (2006).

[73] X. Wang and P. Yang, Journal of visualized experiments:

JoVE (2008).

[74] S. Pagliara, K. Franze, C. R. McClain, G. W. Wylde, C. L. Fisher, R. J. Franklin, A. J. Kabla, U. F. Keyser, and K. J. Chalut, Nature materials **13**, 638 (2014).

[75] T. Pieters and F. Van Roy, J Cell Sci **127**, 2603 (2014).

[76] J. F. Casella, M. D. Flanagan, and S. Lin, Nature **293**, 302 (1981).

[77] T. L. Le, J. L. Stow, *et al.*, The Journal of cell biology **146**, 219 (1999).